Processing and Application of Ceramics 17 [1] (2023) 39–46
https://doi.org/10.2298/PAC2301039Z

High-temperature oxidation behaviour of Si_3N_4 nanowires with different diameters

Shuang Zhao*, Feiyue Yang, Jun Chen, Kunfeng Li, Zhifang Fei, Zichun Yang*

School of Power Engineering, Naval University of Engineering, Wuhan 430033, China

Received 16 August 2022; Received in revised form 8 December 2022; Accepted 19 January 2023

Abstract

α-Si_3N_4 nanowires with diameters of 100–180 nm (Si_3N_4-W1) and 420–510 nm (Si_3N_4-W2) were synthesized by a modified chemical vapour deposition (CVD) method and their microstructure changes after high-temperature oxidation were studied. The results showed that both Si_3N_4 nanowires were not significantly oxidized when the temperature was lower than 900 °C. However, the Si_3N_4-W1 microstructure began to change significantly after oxidation at 1200 °C, while the Si_3N_4-W2 microstructure remained almost unchanged. Moreover, the Si_3N_4-W1 and Si_3N_4-W2 nanowires oxidized significantly after treatment at 1400 °C, with weight gain of 26.4% and 13.7%, respectively.

Keywords: *Si_3N_4 nanowires, vapour deposition, microstructure, high-temperature oxidation*

I. Introduction

Nanowires exhibit unique properties that are different from bulk materials due to quantum and surface effects [1–4]. Properties of Si_3N_4 nanowires such as corrosion resistance, high-temperature resistance, wide band gap, low dielectric loss angle, excellent tensile strength (57 GPa [5]) and toughness (with high modulus of elasticity of 570 GPa [6]) make it a hot spot in current scientific research [7–9]. Si_3N_4 nanowires have great application potential in the fields of reinforced nanomaterials, optoelectronic devices, high-temperature semiconductor materials, super capacitors, etc. [10–13].

Methods used for Si_3N_4 nanowire synthesis mainly include chemical vapour deposition (CVD) method, precursor conversion method, laser ablation method and physical evaporation deposition method. Okamura *et al.* [14] firstly synthesized Si_3N_4 nanowires by electron irradiation pretreatment of polycarbosilane fibres in combination with high-temperature nitridation treatment. Yang *et al.* [15] used amorphous SiCN powder as raw material and obtained Si_3N_4 nanowires and Si_3N_4 nanobelts under the action of Fe-containing catalyst. Bechelany *et al.* [16] synthesized Si_3N_4 nanorods by heating SiC nanowires as templates in NH_3 atmosphere, which realized the conversion of SiC and Si_3N_4 in one-dimensional nanomaterials.

Temperature has a great impact on the properties and application of nanowires, especially for high temperatures [17–21]. On the one hand, the exploration of the high-temperature chemical stability of nanowires is becoming a hot spot of current research. The ultra-light ceramic aerogel prepared by Su *et al.* [22] using SiC nanowires could withstand a high temperature of 900 °C without significant oxidation. Paulowicz *et al.* [23] realized the growth of a new type of flexible and high-temperature stable (≈1400 °C) 3D network material made from interconnected quasi-one-dimensional SnO_2 structure through a simple flame transmission synthesis method. Prakash *et al.* [21] found SiC nanowire grown *in situ* in a carbon fibre play a crucial role in determining oxidation resistance of composite, which can protect the carbon fibres from oxidation at a temperature not exceeding 933 K. On the other hand, the researchers are exploring the changes in the relevant properties of nanowires at high temperatures when they are used in the fields of ferromagnetic response and sensors, etc. For example, by doping InSb nanowires with 2.5% Mn, Hnida *et al.* [20] promoted their robust ferromagnetic response to be retained up to the Curie temperature of nearly 500 K.

In this study, two types of Si_3N_4 nanowires (Si_3N_4-W1 and Si_3N_4-W2) with different diameters were syn-

* Corresponding authors: tel: +86 27 85460570,
e-mail: *zhsh6007@126.com* (S. Zhao)
yangzichun11@sina.com (Z. Yang)

thesized by two modified CVD methods, providing a new method for controlling the Si_3N_4 nanowire diameter. In addition, by comparing and analysing the high-temperature oxidation resistance of these two types of Si_3N_4 nanowires, it may provide a reference for the application of nanowires in high temperature fields.

II. Experimental

Si powder (purity > 99.9%, Forsman Scientific, Beijing, Co. Ltd, China) with a particle size of 3 μm was used as raw material. At first, the Si powder was dried in a vacuum oven for more than 8 h to sufficiently remove moisture (the temperature was set to 80 °C). Next, the dried Si powder was placed into a graphite box, and a graphite plate was placed horizontally about 5 mm above it. When the sample was placed in a nitriding furnace for high-temperature nitriding process, the following two CVD procedures were adopted: i) N_2 (purity was 99.99%, $O_2 \leq 20$ ppm) flowed over the substrate at a flow rate of 40 sccm during the CVD process until the experiment was completed and ii) the furnace was evacuated, then filled with nitrogen and finally the nitrogen pressure was maintained at normal pressure for high-temperature CVD. For convenience, the samples synthesized by the first and second method were denoted as Si_3N_4-W1 and Si_3N_4-W2, respectively. The synthesized samples were nitrided at 1350 °C for 4 h at a heating rate of 2 °C/min.

In high-temperature oxidation resistance experiments the nanowires were placed in a high-temperature furnace and oxidized at a specific temperature (800, 1000, 1200 and 1400 °C) for 2 h in static air conditions. The heating rate was 20 °C/min and the oxidized samples were cooled within the furnace.

The nanowire microstructure was observed via scanning electron microscopy (SEM, Phenom XL, USA) and the elemental composition of the samples was semi-quantitatively analysed using the accompanying energy dispersive spectrometer (EDS). Microstructure was further characterised by using high resolution transmission electron microscopy (HRTEM, Tecnai G2 F30, Netherlands). The phase composition of the samples was determined via X-ray diffraction (XRD, Bruker D8, Germany) with a scanning range of 10° to 45° and the scanning speed 5 °/min. Thermogravimetric analysis of the samples was carried out via synchronous thermal analyser in air atmosphere (TG-DTA, STA 2500, Germany) and up to 1450 °C at a heating rate of 10 °C/min.

III. Results and discussion

3.1. Microstructure and phase composition

The white film-like Si_3N_4 nanowires Si_3N_4-W1 and Si_3N_4-W2 synthesized on the graphite box after the reaction were shown in Figs. 1a and 1b respectively. Figure 1c presents the samples peeled off from the graphite sheet (the above samples all showed good flexibility).

Morphology of the Si_3N_4-W1 and Si_3N_4-W2 nanowires was analysed by SEM (Fig. 2). The results show that the Si_3N_4-W1 sample consists of thin and curved nanowires with a diameter of 100–180 nm (Fig. 2a), while the Si_3N_4-W2 sample has thick and straight nanowires, whose diameters are mainly distributed in the range of 420–510 nm (Fig. 2b). Since there was no catalyst involved in the reaction process, the growth of Si_3N_4 nanowires should conform to the vapour-solid (VS) growth mechanism.

Phase stability diagram in Si-O-N system at 1350 °C is shown in Fig. 3 [24–26]. It reveals that the synthe-

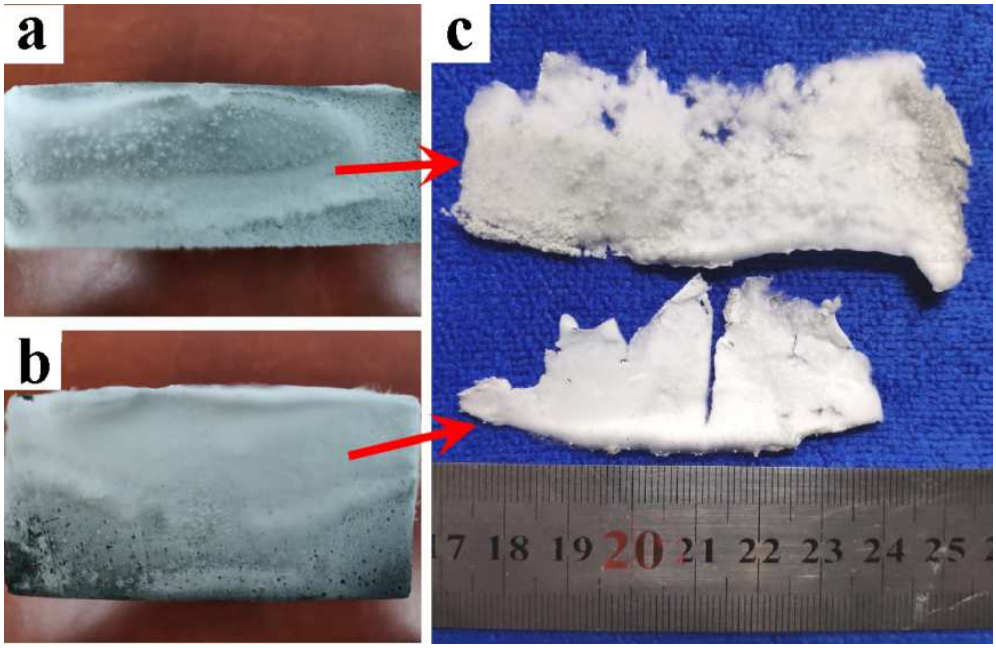

Figure 1. Si_3N_4-W1 (a) and Si_3N_4-W2 (b) samples synthesized on the graphite box after the reaction and images of the samples peeled off from the graphite sheet (c)

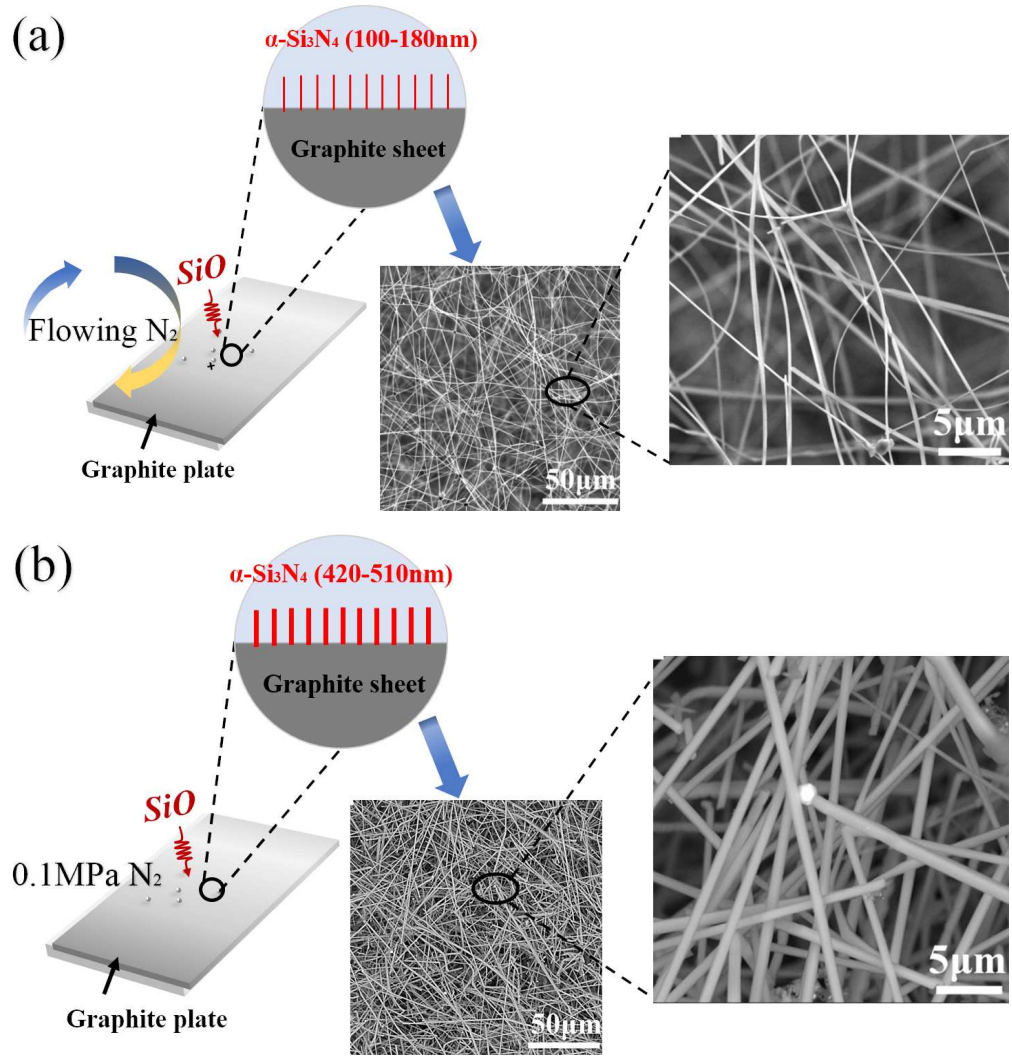

Figure 2. Schematic diagram of the synthesis process of two types of Si_3N_4 nanowires: a) Si_3N_4-W1 and b) Si_3N_4-W2

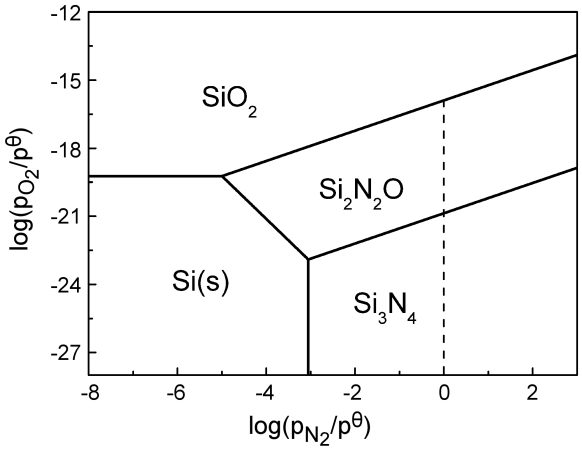

Figure 3. Diagram of the regions where each phase exists stably in the Si-N-O system at 1350 °C

sis of Si_3N_4 phase requires a sufficiently low oxygen partial pressure. Under high temperature conditions, the oxygen impurities in nitrogen might react with C in the graphite devices to form CO (Eq. 1) or react with Si powder to form gaseous SiO (Eq. 2), which promotes the reduction of oxygen partial pressure. Moreover, the amorphous SiO_2 native layer attached to the Si surface can also react with Si to generate gaseous SiO (as an intermediate product in the synthesis of Si_3N_4 nanowires) at high temperatures (Eq. 3) [27–29]. The formed gaseous SiO diffused to the vicinity of the graphite plate and reacted with N_2 to promote Si_3N_4 nucleation (Eq. 4) and then epitaxially grew into nanowires [30–32].

$$C(s) + 0.5\,O_2(g) \longrightarrow CO(g) \quad (1)$$

$$Si(s) + 0.5\,O_2(g) \longrightarrow SiO(g) \quad (2)$$

$$Si(s) + SiO_2(s) \longrightarrow 2\,SiO(g) \quad (3)$$

$$6\,SiO(s) + 4\,N_2(g) \longrightarrow 2\,Si_3N_4(s) + 3\,O_2(g) \quad (4)$$

The observed difference in the diameter of the Si_3N_4-W1 and Si_3N_4-W2 nanowires may be attributed to the changes in N_2 atmosphere conditions in different CVD procedures. In the first CVD method, gaseous SiO was relatively dispersed under the action of flowing N_2, after which it reacted with N_2 and then precipitated to form small nuclei of Si_3N_4, which finally grew into

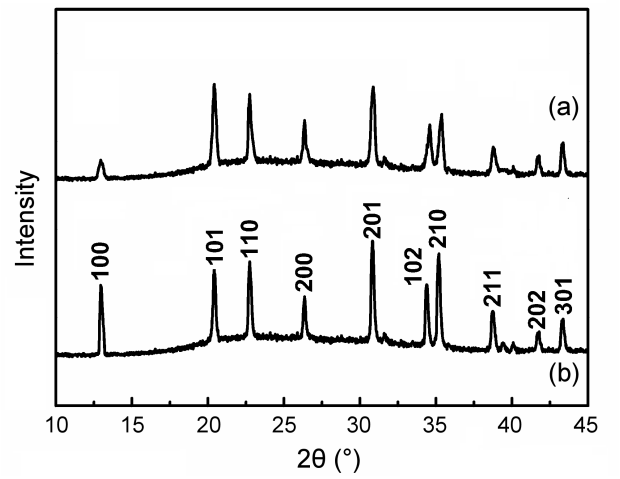

Figure 4. XRD patterns of: a) Si_3N_4-W1 and b) Si_3N_4-W2 nanowires

Si_3N_4 thin nanowires. On the contrary, for the second CVD method, the gas pressure in the furnace might promote the nucleation of Si_3N_4 formed by the reaction of gaseous SiO and N_2 to merge and grow into thick and straight Si_3N_4 nanowires.

XRD results show that the diffraction peaks of both Si_3N_4-W1 and Si_3N_4-W2 nanowires have sharp peaks, indicating that they are all well crystallized (Fig. 4). Moreover, the peak intensity for the XRD diffraction peak corresponding to the (100) crystal plane of the Si_3N_4-W2 is higher than that of the Si_3N_4-W1 sample, indicating that there was a tendency for preferred orientation.

HRTEM images and selected area electron diffraction (SAED) showed that the diffraction spots of the samples are all distributed in a lattice pattern, which further indicated the good crystal structure of the nanowires (Figs. 5b and 5d). The lattice fringe spacing (interplanar spacing) of the Si_3N_4-W1 nanowires with a diameter of 173 nm is 0.43 nm, which grew along the [101] direction, conforming to the standard map of JPCDS card No. 76-1412 (Figs. 5a and 5b). On the other hand, the lattice fringe spacing of the Si_3N_4-W2 nanowires with a diameter of 447 nm is 0.67 nm, and the growth direction was [100], which conformed to the standard map of JPCDS card No. 76-1407 (Figs. 5c and 5d). Hartman and Perdok [33,34] believe that PBC theory can explain the phenomenon that nanowires grow along the preferred orientation. They suggested that there are a series of periodic strong bond chains in crystals, and the crystal grows parallel to the bond chain and grows fastest in the direction of the strongest bond force, thereby

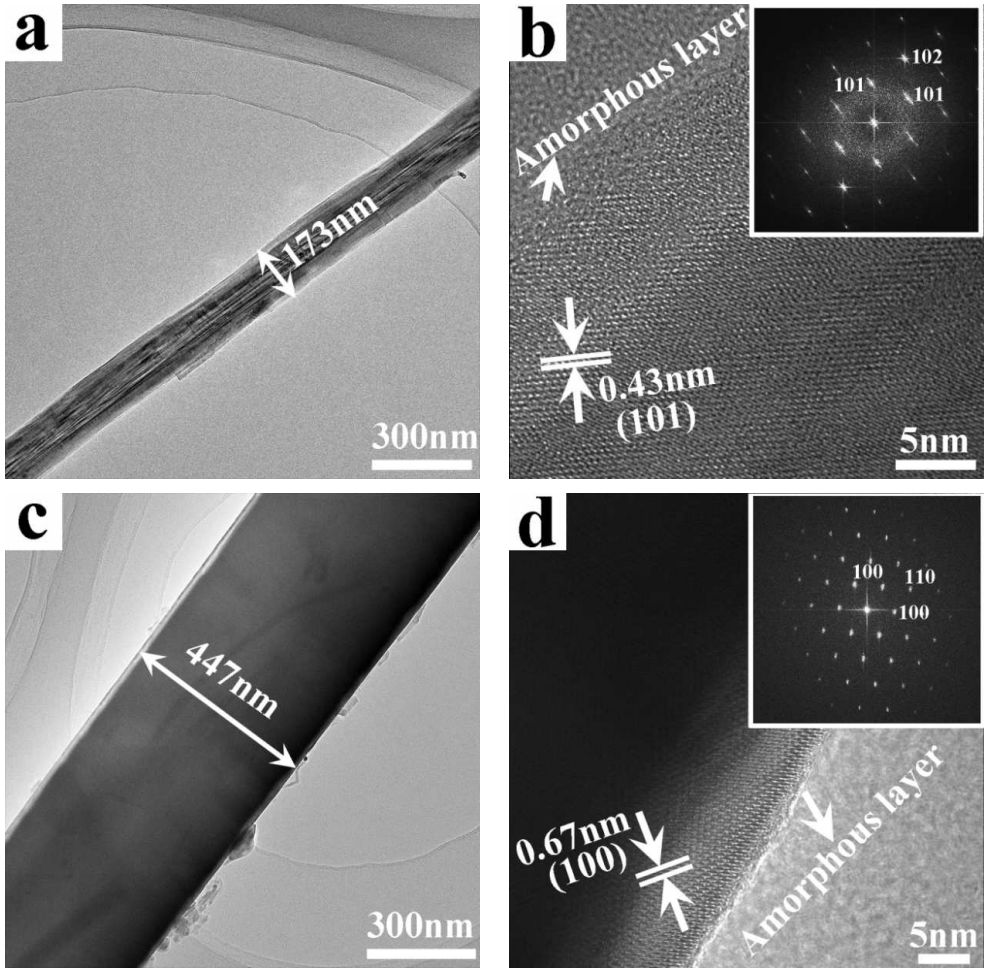

Figure 5. HRTEM images and SAED spectra of Si_3N_4 nanowires synthesized under different nitriding conditions: (a,b) Si_3N_4-W1, (c,d) Si_3N_4-W2

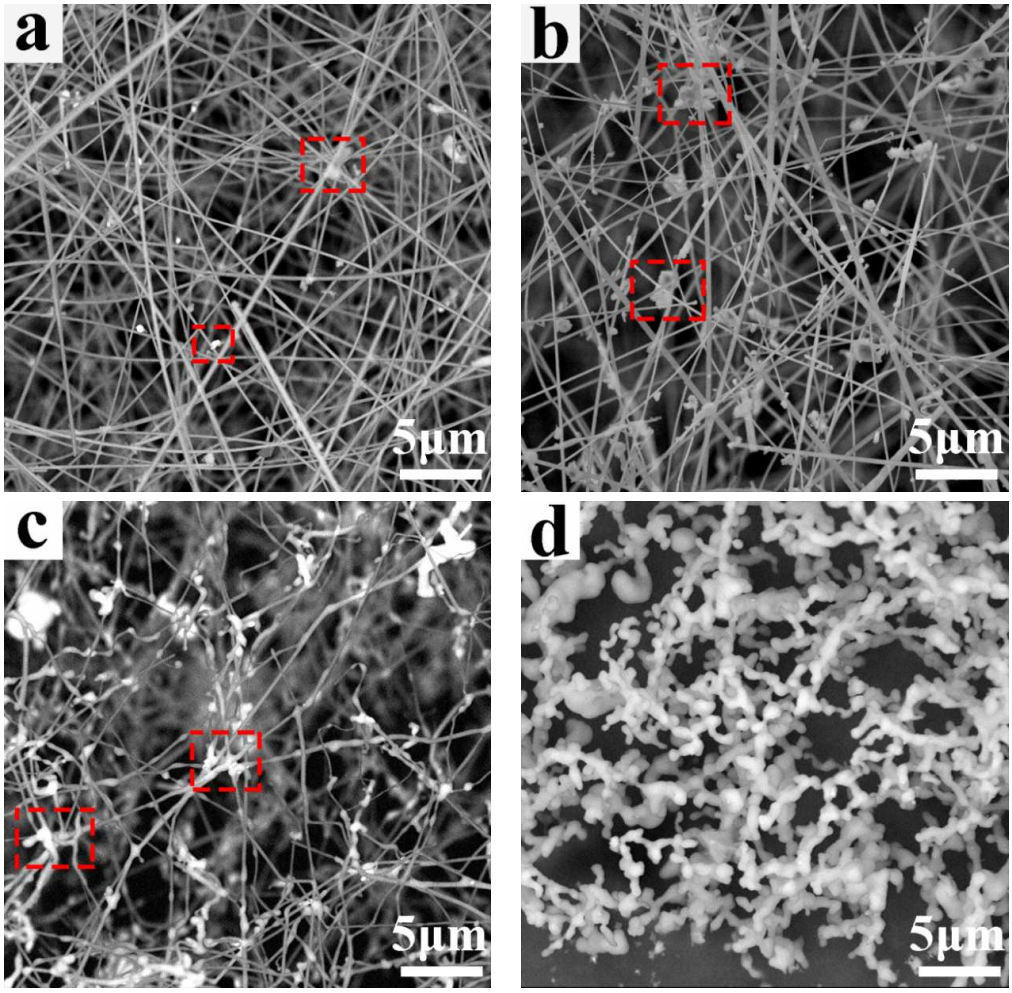

Figure 6. SEM micrographs of Si_3N_4-W1 nanowires after oxidation at different temperatures: a) 800 °C, b) 1000 °C, c) 1200 °C and d) 1400 °C

forming nanowires, nanotubes, etc. As mentioned before, the different interplanar spacing and growth directions of nanowires may be attributed to the differences in the growth process of nanowires when the different CVD methods were used. Nanowires with different microstructural features have been reported to exhibit specific optical, electrical and mechanical properties, which have an important impact on their applications in many fields such as electronic components and optical parts [35]. In addition, the above two types of nanowires have an amorphous thin layer on the surface, which is a normal phenomenon for the synthesised Si_3N_4 nanowires [36,37].

3.2. Nanowires after oxidization

Different sizes of the prepared Si_3N_4 nanowires may exhibit different high-temperature oxidation resistance due to the surface effect. The changes of microstructure and phase composition of two types of nanowires after being oxidized at different temperatures were observed by SEM analyses. SEM images of the Si_3N_4-W1 nanowires after oxidation at different temperatures (800, 1000, 1200 and 1400 °C) in air conditions are shown in Fig. 6. After oxidation at 800 °C, a small amount of droplet-like small particles appeared on the nanowire surfaces. When the oxidation temperature was increased to 1000 °C, the number of droplet-shaped small particles on the nanowires increased significantly and became larger. After being oxidized at 1200 °C, the nanowires appeared to shrink and bend, and the size of droplet-like particles on the nanowires further increased. When the oxidation temperature was increased to 1400 °C, the nanowires further shrank into short branches and no longer exhibited obvious nanowire morphology.

Figure 7 displays SEM micrographs of the Si_3N_4-W2 nanowires oxidized in air at 800, 1000, 1200 and 1400 °C. After oxidation at 800 °C, the microstructure of the nanowires was basically unchanged. When the oxidation temperature was increased to 1000 °C, the intersection of the nanowires began to melt, and a small amount of droplet-like particles began to appear on the nanowire surfaces. After being oxidized at 1200 °C, the melting at the intersection of the nanowires was enhanced and the number of droplets on the nanowires increased. When the oxidation temperature was increased to 1400 °C, the microstructure of the nanowires appeared as a rough bead, but it still obviously remained linear structure.

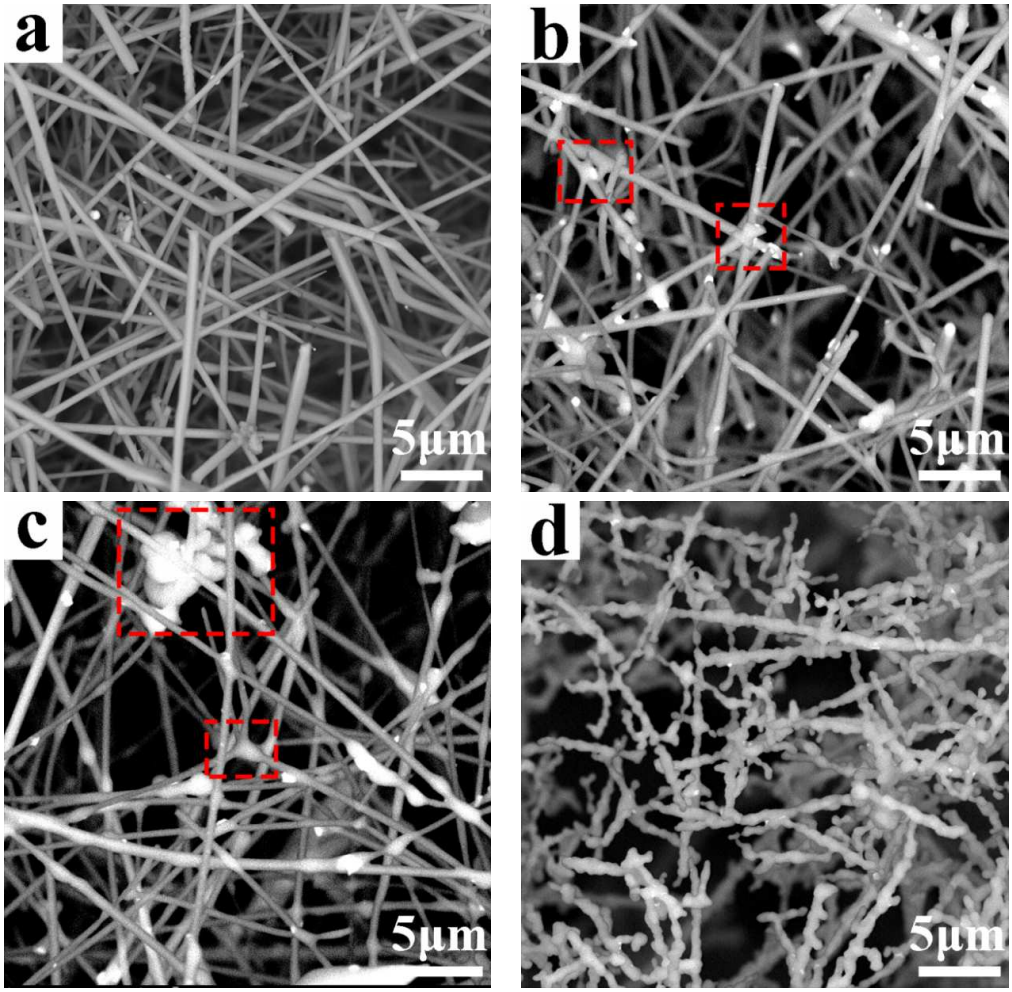

Figure 7. SEM micrographs of Si_3N_4-W2 nanowires after oxidation at different temperatures: a) 800 °C, b) 1000 °C, c) 1200 °C and d) 1400 °C

Nanowires usually exhibit unique properties that are different from bulk materials due to quantum and surface effects [2,3]. Nanowires with small diameter have higher surface energy than others, so they are more likely to melt at high temperatures to produce droplet-like small particles.

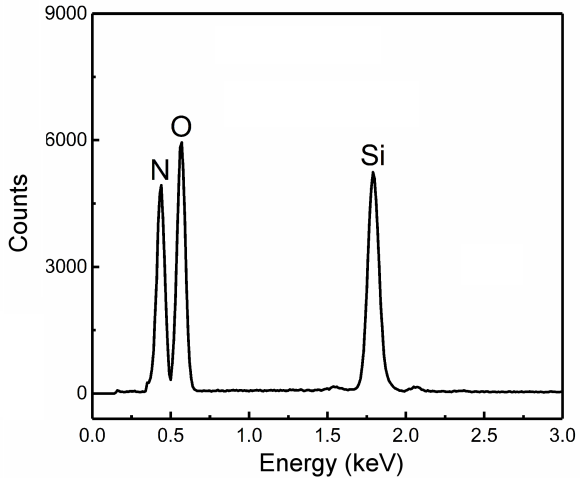

Figure 8. EDS analysis of the droplet-like particle shown in Fig. 7c

The EDS analysis (Fig. 8) of the droplet-like particle in Fig. 7c revealed that it was mainly composed of three elements: Si, N and O. Si_3N_4 can be oxidized with oxygen under high temperature environment, so the presence of O element should be related to the partial oxidation of Si_3N_4. It was found that the microstructure changes of the Si_3N_4-W1 and Si_3N_4-W2 nanowires were small or even unchanged when the oxidation temperature was lower than 800 °C. As the oxidation temperature increased, the microstructure of the Si_3N_4 nanowires began to melt and shrink. Moreover, under the same oxidation conditions, the microstructure of the thick nanowires (Si_3N_4-W2) changed less than that of thin nanowires (Si_3N_4-W1), indicating that the high-temperature oxidation resistance of Si_3N_4 nanowires with larger diameters was significantly better.

3.3. High-temperature oxidation resistance

Figure 9 presents the TG-DTA curves of the Si_3N_4-W1 and Si_3N_4-W2 samples heated in air atmosphere. The results show that when the oxidation temperature was around 300 °C, the TG curves have a slight downward trend (the weight loss of the Si_3N_4-W1 and Si_3N_4-W2 was 3.8% and 1.4%, respectively), and the corre-

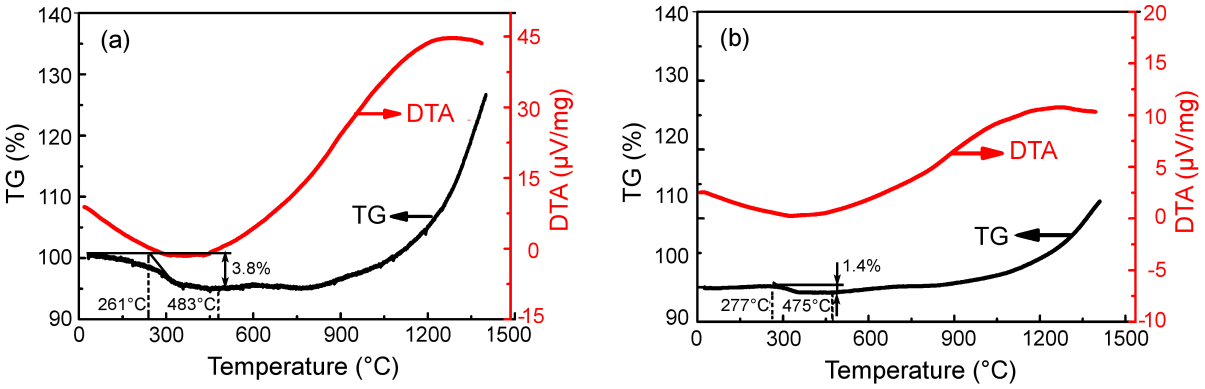

Figure 9. TG-DTA curves of: a) Si_3N_4-W1 and b) Si_3N_4-W2 samples

sponding DTA curves of both samples showed a broad endothermic peak. The above phenomenon might be caused by the heat absorption and evaporation of a small amount of water adsorbed on the nanowires. Compared to the Si_3N_4-W2, the Si_3N_4-W1 sample contained more volatile impurities due to their larger specific surface area, so its weight loss was slightly higher than that of the Si_3N_4-W2. Moreover, with the increase of temperature, the TG curves of both samples generally maintained a relatively horizontal trend up to 900 °C, indicating that they were substantially not oxidized by oxygen at this time.

When the temperature was increased to about 900 °C, the TG curves of both samples began to rise significantly. At these conditions, the rate at which Si_3N_4 nanowires were oxidized to SiO_2 started to accelerate. When the temperature was increased to 1400 °C, the weight gain of the Si_3N_4-W1 and Si_3N_4-W2 nanowires reached 26.4% and 13.7%, respectively (if Si_3N_4 is completely oxidized to SiO_2, the theoretical weight gain of the curve should be 28.6%). The above results indicate that the high-temperature oxidation resistance of the thick nanowires (Si_3N_4-W2) is better than that of the thin nanowires (Si_3N_4-W1) under the same oxidation conditions. This phenomenon can be explained as follows: compared with thick nanowires, thin nanowires have a larger specific surface area and higher surface activation energy, which makes it easier to react with O_2, resulting in relatively weak oxidation resistance properties.

IV. Conclusions

In summary, Si_3N_4 nanowires with diameters of 100–180 nm (Si_3N_4-W1) and 420–510 nm (Si_3N_4-W2) were synthesized by two modified CVD methods. Both Si_3N_4 nanowires crystallized well and their interplanar spacings were 0.43 nm and 0.67 nm, respectively. Comparing the high-temperature oxidation resistance of the Si_3N_4-W1 and Si_3N_4-W2 samples, the results were as follows:

(1) Microstructure of both Si_3N_4 nanowires changed with the increase of oxidation temperature, and when the oxidation temperature was increased to 1400 °C, the Si_3N_4-W1 shrank into short branches, while the Si_3N_4-W2 appeared as a rough bead and still remained a linear structure.

(2) The oxidation rate of both α-Si_3N_4 nanowires started to accelerate significantly when temperature exceeded 900 °C, and after oxidation at 1400 °C the weight gain of the Si_3N_4-W1 and Si_3N_4-W2 reached 26.4% and 13.7%, respectively. By comparing and analysing the high temperature oxidation resistance of the Si_3N_4-W1 and Si_3N_4-W2 samples, it may provide a reference for the application of Si_3N_4 nanowires in the high-temperature field.

Acknowledgment: This work was supported by the National Natural Science Foundation of China (51802347). The authors thank Shiyanjia Lab (www.shiyanjia.com) for the TEM analysis.

References

1. A.P. Schlaus, M.S. Spencer, K. Miyata, F. Liu, X. Wang, I. Datta, M. Lipson, A. Pan, X.-Y. Zhu, "How lasing happens in $CsPbBr_3$ perovskite nanowires", *Nat. Commun.*, **10** [1] (2019) 265.
2. E. Garnett, L. Mai, P. Yang. "Introduction: 1D nanomaterials/nanowires", *Chem. Rev.*, **119** [15] (2019) 8955–8957.
3. P. Sutter, S. Wimer, E. Sutter, "Chiral twisted van der Waals nanowires", *Nature*, **570** [7761] (2019) 354–357.
4. L.Yin, X. Zhou, J. Yu, H. Wang, "Preparation of silicon nitride foam with three-dimensional interconnected pore structure", *Mater. Design.*, **89** [2016] 620–625.
5. G. Brambilla, F. Xu, P. Horak, Y. Jung, F. Koizumi, N.P. Sessions, E. Koukharenko, X. Feng, G.S. Murugan, J.S. Wilkinson, D.J. Richardson, "Optical fiber nanowires and microwires: Fabrication and applications", *Adv. Opt. Photonics*, **1** [1] (2009) 107–161.
6. G. Jing, H. Ji, W. Yang, J. Xu, D.P. Yu, "Study of the bending modulus of individual silicon nitride nanobelts via atomic force microscopy", *Appl. Phys. A*, **82** [3] (2006) 475–478.
7. F. Yang, S. Zhao, Z. Yang, G. Chen, K. Li, Z. Fei, Z. Lou, "Microstructure and properties of Si_3N_4 foam ceramics modified by in-situ self-grown nanowires", *Ceram. Int.*, **45** [14] (2019) 16725–16730.
8. L. Elsinger, R. Gourgues, I.E. Zadeh, J. Maes, A. Guardiani, G. Bulgarini, S.F. Pereira, S.N. Dorenbos, V.

Zwiller, Z. Hens, D. Van Thourhout, "Integration of colloidal PbS/CdS quantum dots with plasmonic antennas and superconducting detectors on a silicon nitride photonic platform", *Nano Lett.*, **19** [8] (2019) 5452–5458
9. W. Hartmann, P.P. Varytis, H. Gehring, N. Walter, F. Beutel, K. Busch, W. Pernice, "Broadband spectrometer with single-photon sensitivity exploiting tailored disorder", *Nano Lett.*, **20** [4] (2020) 2625–2631.
10. J. Li, Y. Li, N. Zhou, W. Xiong, G. Wang, Q. Zhang, A. Du, J. Gao, Z. Kong, H. Lin, J. Xiang, C. Li, X. Yin, X. Wang, H. Yang, X. Ma, J. Han, J. Zhang, T. Hu, Z. Cao, T. Yang, J. Li, H. Yin, H. Zhu, J. Luo, W. Wang, H.H. Radamson, "Study of silicon nitride inner spacer formation in process of gate-all-around nano-transistors", *Nanomaterials*, **10** [4] (2020) 793.
11. A. Karvounis, N. Aspiotis, I. Zeimpekis, J-Y. Ou, C.-C. Huang, D. Hewak, N.I. Zheludev, "Mechanochromic reconfigurable meta surfaces", *Adv. Sci.*, **6** [21] (2019) 1900974.
12. K.B. Iroshika, Y.M.N.D.Y. Bandara, J.W. Nichols, R.B. Chevalier, J.R. Dwyer, "Surveying silicon nitride nanopores for glycomics and heparin quality assurance", *Nat. Commun.*, **9** (2018) 3278.
13. C.F. Fong, Y. Yin, Y. Chen, D. Rosser, J. Xing, A. Majumdar, Q. Xiong, "Silicon nitride nanobeam enhanced emission from all-inorganic perovskite nanocrystals", *Opt. Express*, **27** [13] (2019) 18673–18682.
14. K. Okamura, M. Sato, Y. Hasegawa, "Silicon nitride fibers and silicon oxynitride fibers obtained by the nitridation of polycarbosilane", *Ceram. Int.*, **13** [1] (1987) 55–61.
15. W. Yang, Z. Xie, H. Miao, L. Zhang, H. Ji, L. An, "Synthesis of single-crystalline silicon nitride nanobelts via catalyst-assisted pyrolysis of a polysilazane", *J. Am. Ceram. Soc.*, **88** [2] (2005) 466–469.
16. M. Bechelany, A. Brioude, S. Bernard, G. Ferro, D. Cornu, P. Miele, "Large-scale preparation of faceted Si_3N_4 nanorods from β-SiC nanowires", *Nanotechnology*, **18** [33] (2007) 335305.
17. G.C. He, R.M. Wei, X.L. Zhu, Y.L. Hua, X. Shao, P.W. Zhang, C.Q. Xie, "Effect of temperature dependent electronics surface and grain boundary scattering on resistivity of polycrystalline silver nanowire fabricated by two-beam laser fabrication technique", *Appl. Surf. Sci.*, **488** (2019) 46–50.
18. V. Rouco, C. Navau, N. Del-Valle, D. Massarotti, G.P. Papari, D. Stornaiuolo, X. Obradors, T. Puig, F. Tafuri, A. Sanchez, A. Palau, "Depairing current at high magnetic fields in vortex-free high-temperature superconducting nanowires", *Nano Lett.*, **19** [6] (2019) 4174–4179.
19. M.J. Martinez-Perez, P.J. Pablo-Navarro, B. Mueller, R. Kleiner, C. Magén, D. Koelle, J.M. de Teresa, J. Sesé, "NanoSQUID magnetometry on individual as-grown and annealed Co nanowires at variable temperature", *Nano Lett.*, **18** [12] (2018) 7674–7682.
20. K.E. Hnida, A. Zywczak, M. Sikora, M. Marciszko, M. Przybylski, "Room-temperature ferromagnetism in InSb-Mn nanowires", *Nano Lett.*, **19** [10] (2019) 7144–7148.
21. J. Prakash, P.S. Sarkar, J. Bahadur, K. Dasgupta, "Effect of in-situ grown SiC nanowire and dense SiC on oxidation resistance of carbon fiber/SiC nanowire/SiC matrix composite in high temperature atmospheric environment", *Corros. Sci.*, **135** (2018) 46–56.
22. L. Su, H. Wang, M. Niu, X. Fan, M. Ma, Z. Shi, S.-W. Guo, "Ultralight, recoverable, and high-temperature-resistant SiC nanowire aerogel", *ACS Nano*, **12** [4] (2018) 3103–3111.
23. I. Paulowicz, V. Hrkac, S. Kaps, V. Cretu, O. Lupan, T. Braniste, V. Duppel, I. Tiginyanu, L. Kienle, R. Adelung, Y.K. Mishra, "Three-dimensional SnO_2 nanowire networks for multifunctional applications: From high-temperature stretchable ceramics to ultraresponsive sensors", *Adv. Electron. Mater.*, **1** [8] (2015) 1500081.
24. S. Farhan, R. Wang, K. Li, "Physical, thermal and ablative performance of CVI densified urethane-mimetic SiC preforms containing in situ grown Si_3N_4 whiskers", *J. Eur. Ceram. Soc.*, **37** [2] (2017) 499–508.
25. U.J.T.O. Linus. "Role of Si_2N_2O in the passive oxidation of chemically-vapor-deposited Si_3N_4", *J. Am. Ceram. Soc.*, **75** [11] (1992) 2995–3000.
26. Z. Chai, J. Ding, C. Deng, H. Zhu, G. Li, C. Yu, "Ni-catalyzed synthesis of hexagonal plate-like alpha silicon nitride from nitridation of Si powder in molten salt media", *Adv. Powder Technol.*, **27** [4] (2017) 1637–1644.
27. P. Yang, C.M. Lieber. "Nanorod-superconductor composites: A pathway to materials with high critical current densities", *Science*, **273** (1996) 1836–1840.
28. Z. Hu, T. Zhu, W. Wu, Z. Peng, F. Hu, Z. Xie, "Growth mechanism of α-Si_3N_4 submicron rods prepared from amorphous Si_3N_4 powders", *Ceram. Int.*, **44** [17] (2018) 22003–22007.
29. B. Wang, X. Huang, X.N. Zhou, Q. Zhi, L.-C. Hao, Z.-X. Li, S. Zhao, B.-Q. Hou, J.-F. Yang, K. Ishizaki, "Synthesis and carbothermal nitridation mechanism of ultra-long single crystal α-Si_3N_4 nanobelts", *Nanotechnology*, **31** (2020) 194001.
30. W. Wang, D. Yao, H. Liang, Y. Xia, K. Zuo, J. Yin, Y.-P. Zeng, "Enhanced thermal conductivity in Si_3N_4 ceramics prepared by using ZrH_2 as an oxygen getter", *J. Alloys Compd.*, **855** [2] (2021) 157451.
31. G. Topateş, "Direct production of Si_3N_4 foams by carbothermal reduction and nitridation of SiO_2", *Ceram. Int.*, **44** [16] (2018) 20545-20550.
32. M. Hnatko, M. Hičák, M. Labudová, D. Galusková, J. Sedláček, Z. Lenčéš, P. Šajgalík, "Bioactive silicon nitride by surface thermal treatment", *J. Eur. Ceram. Soc.* **40** [5] (2020) 1848–1858.
33. F. Fuchs, M.B. Khan, D. Deb, D. Pohl, J. Schuster, W.M. Weber, U. Mühle, M. Löffler, Y.M. Georgiev, A. Erbe, S. Gemming, "Formation and crystallographic orientation of $NiSi_2$-Si interfaces", *J. Appl. Phys.*, **128** [8] (2020) 085301.
34. H. Schneider, J. Schreuer, B. Hildmann. "Structure and properties of mullite - A review", *J. Eur. Ceram. Soc.*, **28** [2] (2008) 329–344.
35. A.I. Hochbaum, P. Yang. "Semiconductor nanowires for energy conversion", *Chem. Rev.*, **110** [1] (2009) 527–546.
36. W. Yang, H. Wang, S. Liu, Z. Xie, L. An, "Controlled Al-doped single-crystalline silicon nitride nanowires synthesized via pyrolysis of polymer precursors", *Phys. Rev. B*, **111** [16] (2007) 4156–4160.
37. X. Ma, K. Zhang, H. Cheng, Z. Chen, F. Wang, S.Z. Li, "Fabrication of self-separable Si_3N_4 microfibers via one step carbothermal reduction and nitridation of rice straw", *Ceram. Int.*, **46** [18] (2020) 29244–29248.